MICROSTRUCTURE, MECHANICAL PROPERTIES AND FATIGUE RESISTANCE OF HIGH CARBON TENSILE WIRES USED IN FLEXIBLE PIPES FOR OFF-SHORE OIL AND GAS TRANSPORTATION

Thaís M. dos Santos[1], Fernanda C.S.C. dos Santos[2], Sérgio S.M. Tavares[1,3*], Rodrigo V. Landim[4] and Javier A.C. Velasco[5]

1 - Departamento de Engenharia Mecânica e de Materiais, Centro Federal de Educação Tecnológica Celso Suckow da Fonseca (CEFET-RJ), Rio de Janeiro, RJ
2- CENANO, Instituto Nacional de Tecnologia (INT), Rio de Janeiro, RJ
3- Programa de Pós-graduação em Montagem Industrial, Universidade Federal Fluminense (UFF), Rua Passo da Pátria, 156, CEP 24210-240, Niterói, RJ.
ssmtavares@id.uff.br
4- Laboratório de H_2S, Instituto Nacional de Tecnologia (INT), Rio de Janeiro, RJ

ABSTRACT

Tensile armour carbon steel wires are structural elements assembled in the complex construction of flexible pipes used in the oil and gas industry. Recently, failures of flexible pipes were associated to tensile armour fractures. Manufacturers do not provide information about the materials and their production flow. In the present work a tensile wire made of cold rolled high carbon steel was characterized. The microstructure and mechanical properties were measured and analyzed. S-N fatigue curve of the wire was constructed and the endurance limit ($S_{e\text{-}0.1}$) for R=0.1 was determined. The endurance limit for for R= -1 was estimated using the Goodman's criteria.

Keywords: *tensile armour, fatigue resistance, high strength-high carbon steel*

INTRODUCTION

Flexible pipes for oil and gas transportation in the off shore production are complex structures made of multiple layers and materials (polymers and metals)(1). The material studied in this work is a high carbon steel (0.65-0.8%C) used in the tensile armour of the flexible pipes. This material must have high yield and ultimate strengths, but not only. High toughness and fatigue resistance are other key properties for this application. Due to several failures of tensile armour elements in service in Brazilian sub-salt fields, they are now being studied in respect to different fracture mechanisms, such as brittle fracture, fatigue and stress corrosion cracking (SCC).
The microstructure and properties of nearly eutectoid steels may vary significantly with the thermomechanical treatment applied, as investigated in several previous works.(2-6)
The exact production flux of the tensile armours depends on the final mechanical properties required and is also a choice of the manufacturers. However, it can be inferred that the material is hot rolled, heat treated, cold drawn, cold rolled, stress relieved, and coiled. The heat treatment before cold deformation can be patenting with isothermal transformation around 500-540ºC,

spheroidization, normalizing, or even quenching and tempering. The final mechanical resistance will be consequence of the heat treatment and cold deformation parameters. Also, a stress relief treatment at temperatures around 400-450^{o}C after cold deformation can be applied. Once in the flexible pipe producer, the wire is un-coiled and pass through a sequence of bending operations in the production line. In this work, a high strength carbon steel for tensile armour, fabricated by a word company in Brazil, was studied in a condition before the processing in the flexible pipe production line.

MATERIALS AND METHODS

The chemical composition of the wire studied is shown in Table 1. According to the manufacturer, the wires passed through hot rolling, patenting heat treatment, cold drawning and rolling, and a final stress relief treatment.
Tensile curves were obtained in duplicate with non-standardized specimens (S1 and S2) with total lenght L=15 mm, as shown in Fig 1. These specimens were not machined, just cut from the as received wire. The cross section area was 80.79 mm^2. The tests were conducted in a servo mechanical INSTRON 5582 with load cell 100kN. Specimens were tested with clip gauge of 25 mm, and with 0.5 mm/min velocity. The true stress (σ)-true strain (ε) curves were fitted and modelled by three equations, Hollomon [(7)], Ludwik [(8)], and Voce [(9)], respectively.

$$\sigma = K_H \cdot \varepsilon^{n_H} \qquad \text{(A)}$$

$$\sigma = \sigma_o + K_L \cdot \varepsilon^{n_L} \qquad \text{(B)}$$

$$\sigma = \sigma_o + a \cdot \varepsilon + b\big(1 - \exp(-c \cdot \varepsilon)\big) \qquad \text{(C)}$$

Where K_H, K_L, n_H and n_L are the resistance parameter and work hardening exponent, respectively, in equations (A) and (B), and a, b and c are independent parameters in (C). Also, in equations (B) and (C), σ_o is the exact point where plastic flow begins.

Table 1: Chemical composition of the wire

C	Mn	P	S	Si	Cu	Al
0.693	0.770	0.014	0.001	0.196	0.013	0.052

Vickers hardness with load 10kgf was measured in the main surface of the wire.
Specimens for fatigue tests had the same geometry and dimensions of tensile specimens (Fig.1). They were not machined nor grinded, i.e. the surface finishing of these specimens was that supplied by the steelmaker. The absolute roughness (R_a) of each specimen was measured with digital surface roughness tester Digimess TR200. The fatigue curve was constructed with four point bend loading tests runed in a servo-hydraulic machine MTS Landmark with frame capacity 25 kN. An apparatus for four point bend test was constructed and assembled in the machine. The specimens were instrumented with two strain gauges to measure the deformation, which was converted to stress using the Hooke's law. The stress ratio ($R=\sigma_{min.}/\sigma_{max.}$) was 0.1, and the frequency 5 Hz. Eight alternate stress levels were used (between 650 and 1000MPa), with at least three specimens per level. The stress amplitude (S_a) versus number of cycles to failure (N_f) curve was constructed using the methodology described in ASTM E-370-10 [10]. Equation (D) representing the S-N curve was fitted.

$$S_a = a + b\left(\log N_f\right) \qquad \text{(D)}$$

Where N_f is the number of cycles to failure; S_a is the Stress amplitude; a and b are constants in the material and in the test conditions.
After the mechanical tests, some fractures were observed in the scanning electron microscope (SEM). The microstructure was also analyzed in the SEM with specimens etched with nital 2%.

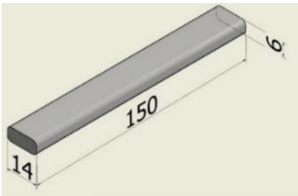

Figure 1: Specimen for tensile test and fatigue tests in mm

RESULTS AND DISCUSSION

The microstructure of the wire is extremely fine, as shown in Figure 2(a-c). Although majoritarily pearlitic (P), other constituents such as poligonal ferrite (PF), upper bainite (UB) and regions with very fine fragmented and spherodized carbides (SC) are also observed. Regions with fine carbides precipitated in the ferrite may be classified as granular bainite (GB). Cold working after patenting promoted the deformation of pearlite and bainite. Beside this, the cold deformation also caused fragmentation of the cementite, as observed by Brito et al[4].Other effect of cold deformation of the patented steels is the reduction of the lamelar spacing, as also reported by Khanchandani and Banerjee[5]. The stress relief treatment after drawning and rolling may have contributed in some degree to spheroidization of fragmented Fe_3C particles. Fig.2(d) shows fragmented and spheroidized Fe_3C carbides with 100 to 200nm of size. Ko et al.[11] showed that the kinetics of speheroidization of Fe_3C is increased by the increase of cold deformation by drawning and shear drawning before heat treatment at 700°C.

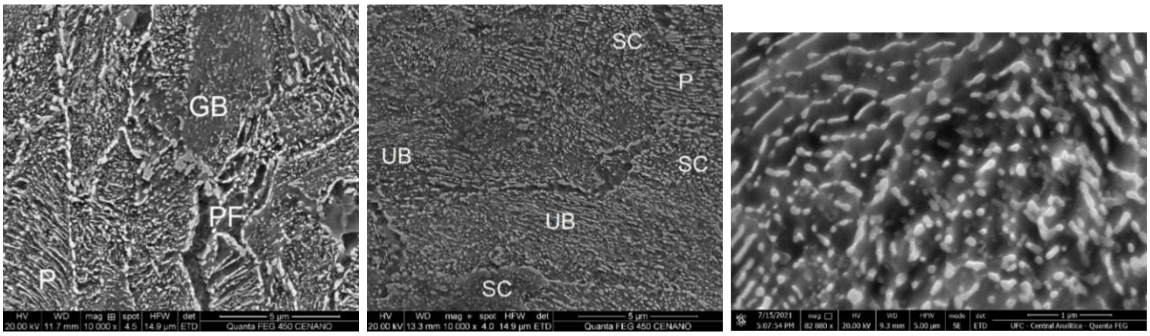

(a) (b) (c)
Figure 2: Microstructure of the steel: (a) side plan (b-c) transversal plane.

Fig. 3(a) shows an example of tensile engineering curve obtained (specimen S1). The 0.2% offset yield limit (σ_Y), the ultimate strength (S_{UTS}), total (ε_T) and uniforme longations (ε_U) are presented in Table 2. The results are compared to those of Rastegary et al.[6] with an eutectoid steel heat treated to produce different multi-constituents microstructures, from spheroidite to bainite. Before cold deformation, the steel investigated in the present work had a microstructure of fine pearlite, bainite and some pro-eutectoide ferrite produced by patenting. The material was then cold drawn and rolled. By comparison with the results of Rastegary et al.[6] , the effect of these cold working operations on the mechanical properties was the increase of yield strength (σ_Y) with much less procounced increase of ultimate (S_{UTS}), which is an expected result for strengthening by work hardening. The true stress-true strain curves for both specimens tested were modeled with equations (A), (B) and (C). Table 3 presents the results of modeling with respective correlation coefficients R^2. Hollomon and Ludwik equations resulted in R^2 coefficients higher than 0.950, which is considered satisfactory. However, the more complex equation of Voce gave the best fitting, with R^2= 0.989 for both specimens tested. The three models are compared to experimental data of specimen S1 in Fig. 3(b).

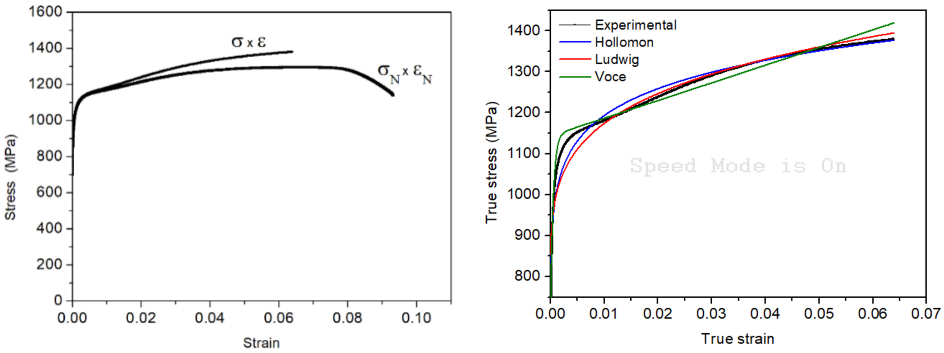

(a) (b)

Figure 3: (a) Engineering curve of specimen S1; (b) True stress versus true strain curve of S1.

Figs.4(a-c) show the macro of the fractured surface of the tensile specimen S1 (S2 shows similar behavior). In the macrography several parallel macro cracks are observed. These cracks indicate a brittle behavior. In the SEM analysis (Figs. 4(b-c)) the central area has dimples of small size, also indicating a brittle behavior, in agreement to the low ductile parameters in the tensile tests.

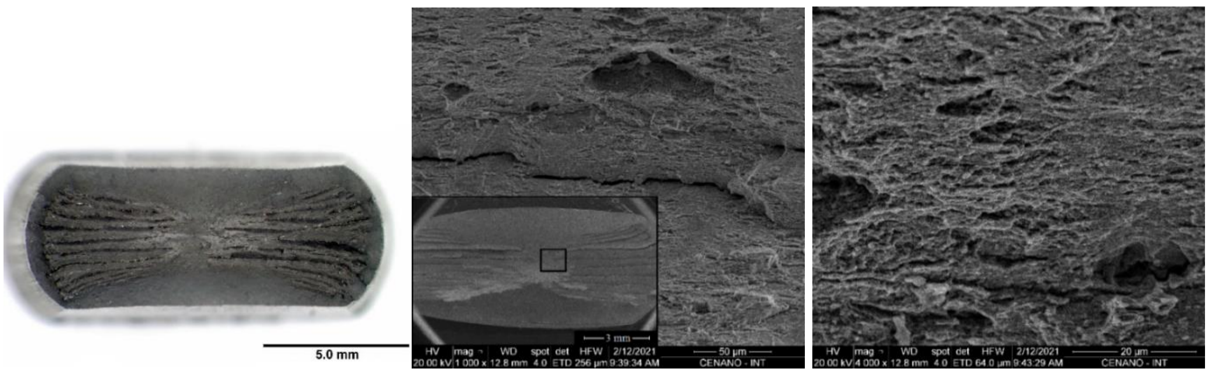

Figure 4: (a) Macro of the fracture surface of specimen S1 after tensile tests (b-c) SEM images of the central part of the fracture of specimen S1, showing cracks (b) and micro dimples (c).

Table 2: Tensile mechanical properties of the wire

Specimen	σ_Y (MPa)	S_{UTS}(MPa)	σ_Y/S_{UTS}	Elongation (%)		Area Reduction (%)
				Total	Uniform	
S1 (this work)	1104	1296	0.85	9.3	7.1	31.5
S2 (this work)	1120	1295	0.86	9.5	7.0	31.5
B [3]*	995	1377	0.72	9.0	7.0	25.0
B + P [3]*	935	1350	0.69	12.0	8.0	33.0
VFP [3]*	762	1207	0.63	13.0	8.0	36.0
PF + FP [3]*	796	1182	0.67	12.0	9.0	39.0
CP [3]*	583	1057	0.55	12.0	9.0	27.0
PS + FP [3]*	615	1041	0.59	21.0	13.0	59.0
SC [3]*	518	871	0.59	27.0	17.0	54.0

* In reference to Rastegary et al.[3]: B=Bainite; P=Pearlite; PF=Pro-Eutectoide ferrite; FP=Fine Pearlite; VFP=Very Fine Pearlite; CP=Coarse Pearlite; PS=Partially Spheroidized; SC=Spheroidized Cementite.

Table 3: Modelling parameters for Hollomon [1] Ludwik [2] and Voce's [3] equations and R^2.

Specimen	Model	σ x ε modelled equation (MPa)	R^2
S1	Hollomon	$\sigma = 1702.8 \cdot \varepsilon^{0.077}$	0.978
	Ludwik	$\sigma = 703 + 1223.2 \cdot \varepsilon^{0.207}$	0.953
	Voce	$\sigma = 703 + 4312.2 \cdot \varepsilon + 440.3 \cdot (1-\exp(-1971.4 \cdot \varepsilon))$	0.989
S2	Hollomon	$\sigma = 1631.4 \cdot \varepsilon^{0.066}$	0.979
	Ludwik	$\sigma = 841 + 1084.0 \cdot \varepsilon^{0.248}$	0.972
	Voce	$\sigma = 841 + 4448.8 \cdot \varepsilon + 303.4 \cdot (1-\exp(-1525.7 \cdot \varepsilon))$	0.989

The average roughness of the specimens used for the construction of the S-N curve was 1.01±0.19µm, and the S-N curve is shown in Fig. 5. The best curve and the lines for a confidence interval of 95% were plotted.

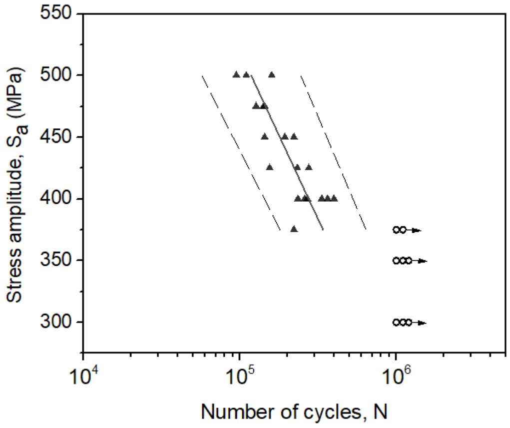

Figure 5: S-N curve for R=0.1

Two specimens tested with Sa = 375 MPa and all specimens tested with $S_a \leq$ 350 MPa did not fail. It is possible to estimate conservatively that the endurance limit for R=0.1 is 350 MPa. Eq. (E) based on the Goodman's relation[12] was used to estimate the endurance limit for R=-1.

$$S_e = \frac{\left(\frac{S_e^*}{S_{UTS}}\right) \cdot \left(\frac{(1-R)}{(1+R)}\right) \cdot S_{UTS}}{\left(\frac{(1-R)}{(1+R)}\right) \cdot \frac{S_e^*}{S_{UTS}}} \qquad \text{(E)}$$

Where S_e is the endurance limit for R=-1, S_e* is the endurance limit for R≠-1 and S_{UTS} is the ultimate strength. For R=0.1, applying S_e*= 350MPa and S_{UTS}=1295 MPa, the S_e obtained is 574MPa, which represents 44% S_{UTS}.

The fracture surfaces of specimens tested with amplitude stresse (σ_a) 400MPa, 450MPa and 500 MPa were analyzed in the SEM (Fig. 6(a-c)). These three specimens showed very similar features. Cracks and ratchet marks are observed with low magnification, as shown in Fig.6(a). In the microscopic scale it is possible to observe several microcracks and tearing (Fig, 6(b)). Fig. 6(c) show regions with striations, but they are more rarely observed than the microcracks and tearing events in the fracture surface. According to Dieter [12] and Das [13] striation is difficult to observe in high strength steels. Nejad et al.[14] studied the fatigue resistance of a nearly eutectoid rail steel, and observed a complex fracture surface, with secondary cracks striations and cleavage facets. Toribio et al.[15] reported tearing events in a spheroidized steel.

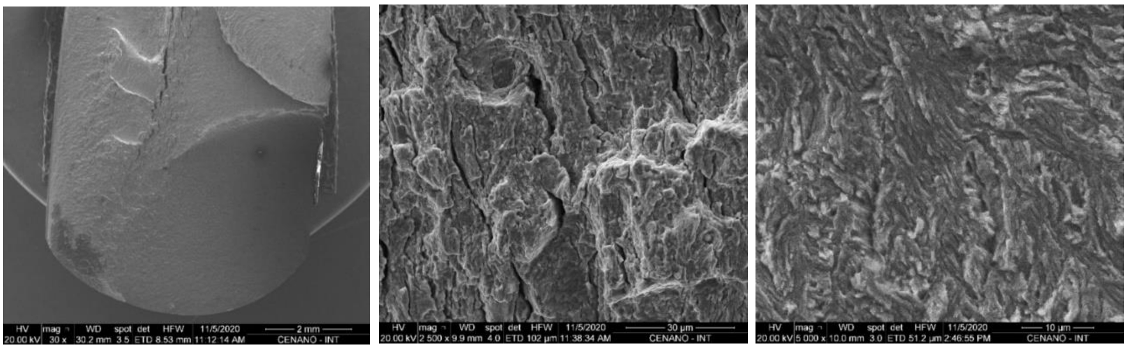

(a) (b) (c)

Figure.6: Fractographic analysis of fatigue specimens: (a) σ_a = 450MPa, showing cracks and ratched marks; (b) σ_a = 450MPa, showing microcracks and tearing; (c) σ_a = 450MPa, showing striation.

CONCLUSIONS

The mechanical properties and microstructure of a high carbon (0.69%C) high strength steel for tensile armour wires of flexible pipes were investigated. The material has been hot rolled, patented, cold worked by rolling and drawning, and stress relieved. The microstructure which resulted from these operations was composed by deformed pearlite, upper and granular bainite. The cold working and stress relief provoked the fragmentation and speroidization of very fine carbides (Fe_3C). The tensile properties of the material were typical of cold worked steel, and the flow stress curve was modeled with Hollomon's, Ludwig's and Voce's equations, with best results obtained in the last one. The S-N curve for R=0.1 was determined, and then durance limit was conservatively estimated in 350MPa. Using the Goodman's relation the endurance limit for R=-1 (Se) was estimated as 574MPa, which is 44% of the ultimate strength.

AKNOWLEDGEMENTS

Authors acknowledge MCTI/SISNANO/INT-CENANO-CNPq (grant 442604/2019) for SEM.

REFERENCES

(1) Duy-Hung Mac, Paul Sicsic, Procedia Engineering 213 (2018) 708-719.
(2) M.V. Chukin, N. V. Koptseva, Yu. Yu. Efimova, D. M. Chukin, O. A. Nikitenko, Steel in Translation 48(4) (2018) 224-228.
(3) R. L. Plaut, A.F. Padilha, N.B. Lima, C. Herrera, A. F. Filho, L. H. Yoshimura, Materials Science and Engineering A 499 (2009) 337–341.
(4) Y.C. Brito, B. W. Ramos, S.V. Junior, R.S. Namur, O.M. Cintho, Equal Channel Angular, Materials Sience Forum 1012 (2020) 360-365.
(5) H. Khanchandani, M.K. Banerjee, J. of Mat. and Eng. and Performance 27(1) (2018) 261-270.
(6) H. Rastegari, A.Kermanpur, A.Najafizadeh, Mat. Sci. Eng. A 632 (2015) 103–109.
(7) J.H. Hollomon, Tensile Deformation, Trans. AIME 162, 268-290 (1945).
(8) P. Ludwik, Elemente der Technologishen Mechanic. Ver Julius Springer 32, (1909).
(9) S.M. Kraft, A. P. Gordon, , Textile Research Journal, v. 00, pp. 1-24, 2011.
(10) ASTM E739-10 - Standard Practice for Statistical Analysis of Linear or Linearized Stress-Life (S-N) and Strain-Life (ε-N) Fatigue Data, ASTM International, 2010.
(11) Y.G. Ko, S. Namgung, D.H. Shin, I.H. Son, K.H. Rhee, Duk-Lak L. Ko, J.MaterSci. 45 (2010) 4866–4870.
(12) G.E. Dieter, D. Bacon, Mechanical Metallurgy, McGraw-Hill, 1988.
(13) A.K. Das, Metallurgy of Failure Analysis (McGraw Hill, New York, 1996)
(14) R. M. Nejad, M. Shariati, K. Farhangdoost, Theor. and App. Fract. Mech. 101 (2019) 320-331.
(15) J. Toríbio, B. González, J.C. Matos, Procedia Structural Integrity 28 (2020) 2378–238.